

Ga adsorption and desorption kinetics on M -plane GaN

Oliver Brandt,* Yue Jun Sun, Lutz Däweritz, and Klaus H. Ploog
Paul-Drude-Institut für Festkörperelektronik, Hausvogteiplatz 5–7, D-10117 Berlin, Germany
 (Received 3 December 2003; published 30 April 2004)

We study the adsorption and desorption kinetics of Ga on GaN($1\bar{1}00$) in molecular-beam epitaxy using *in situ* reflection high-energy electron diffraction. Two stable surface phases are identified, which manifest themselves at low temperature by a $(1\times 2)/(4\times 2)$ reconstruction at bilayer coverage and a (4×4) reconstruction at trilayer coverage. At growth temperature, Ga adsorbs layer-by-layer up to bilayer coverage after which Ga cluster and eventually droplet formation occurs. The bilayer desorption is delayed by “feeding” from this excess Ga. The optimum growth conditions with regard to surface morphology are those giving rise to trilayer coverage at low temperature. This finding is in contrast to the case of GaN(0001) where the optimum growth conditions are related to the formation of a Ga bilayer at the growth front.

DOI: 10.1103/PhysRevB.69.165326

PACS number(s): 68.43.Mn, 81.15.Hi, 61.14.Hg, 68.35.Bs

I. INTRODUCTION

Group-III nitrides are inherently piezoelectric and pyroelectric materials due to their wurtzite structure. Since the polar axis in the wurtzite lattice is the $[0001]$ direction (the c axis), large electrostatic fields may arise in heterostructures grown along this orientation. However, structures grown along any direction perpendicular to $[0001]$, such as $[1\bar{1}00]$ (M plane) and $[11\bar{2}0]$ (A plane), are free of both piezoelectrical and pyroelectrical polarization along the growth direction.¹ The resulting absence of electrostatic fields constitutes a distinct advantage for fabricating high-efficiency GaN-based light-emitting diodes over corresponding $[0001]$ -oriented structures on conventional substrates such as Al_2O_3 (0001) and SiC (0001). Additionally, since the c axis of GaN lies in the growth plane for the nonpolar directions, the optical properties of these structures are inherently strongly anisotropic,² making them promising candidates for polarization-sensitive photodetectors.³ Consequently, the growth of group-III nitrides along nonpolar orientations, such as $[1\bar{1}00]$ (Refs. 4–9) and $[11\bar{2}0]$,^{10–12} has recently attracted considerable attention.

However, the optimum growth conditions for any of these nonpolar orientations have yet to be explored. This fact is in contrast to the case of GaN(0001), for which several studies have established these conditions in molecular-beam epitaxy (MBE) and related them to the existence of a Ga bilayer on the growth front.^{13–17} This Ga bilayer is predicted by density-functional calculations to consist of a bottom Ga monolayer (ML) commensurate to the Ga-terminated GaN(0001) surface, and a laterally contracted, incommensurate top Ga ML.¹⁴ This structure was found to be stable under Ga-rich conditions due to the reduced Ga-Ga spacing in the top layer which is predicted to be close to that of bulk Ga. The total amount of Ga contained within this structure is 2.3 ML (1 ML = 1.136×10^{15} Ga adatoms cm^{-2} on GaN(0001)). The lateral mobility of the Ga atoms within the bilayer is predicted to be high, consistent with the high morphological quality of GaN(0001) grown under conditions giving rise to bilayer coverage. A direct experimental evidence for the presence of this bilayer is obtained by reflection

high-energy electron diffraction (RHEED). GaN layers grown under Ga-stable conditions exhibit a dim (1×1) RHEED pattern during growth, but when quenched to temperatures below 300 °C, diffuse “sidebands” with a spacing slightly larger than the first-order bulk streaks are observed.¹⁷ This spacing corresponds exactly to the theoretically predicted Ga-Ga spacing in the laterally contracted top ML of the Ga bilayer structure.

For GaN($1\bar{1}00$), such a detailed understanding of the surface structure in MBE is lacking. Empirically, we have found that Ga-rich conditions^{18,19} result in GaN($1\bar{1}00$) layers with comparatively smooth surface morphology, whereas N-rich conditions lead to a severe roughening of the growth front. Recently, Lee *et al.*²⁰ observed a reconstruction of approximate symmetry “ (4×5) ” on Ga-rich grown GaN($1\bar{1}00$) on ZnO by scanning tunneling microscopy. The surface was found to be metallic in nature, and the authors proposed that it consists of ≥ 2 ML [1 ML = 1.21×10^{15} Ga adatoms cm^{-2} on GaN($1\bar{1}00$)] of Ga. This proposal is based on density-functional calculations predicting that Ga-adlayer structures with (1×1) symmetry and coverages between 2 and 3 ML on GaN($1\bar{1}00$) are energetically favorable under Ga-rich conditions.²⁰

In this paper, we present a comprehensive study on the adsorption and desorption kinetics of Ga on GaN($1\bar{1}00$) using *in situ* RHEED. Two stable surface phases are identified, which manifest themselves at low temperatures by a $(1\times 2)/(4\times 2)$ reconstruction at bilayer coverage and a (4×4) reconstruction at trilayer coverage. At high temperature, Ga adsorbs layer-by-layer up to bilayer coverage after which condensation of excess Ga occurs. For very Ga-rich conditions, this excess Ga ripens into Ga droplets. The bilayer desorption is counteracted by “feeding” from excess Ga. The optimum growth conditions with regard to surface morphology are those giving rise to trilayer coverage at low temperature.

II. EXPERIMENT

All studies were carried out in a custom-designed, solid-source three-chamber MBE system equipped with a water-

cooled radio-frequency plasma source (EPI Uni-Bulb™) to provide atomic nitrogen. The N source, operating at a plasma power of 400 W with a N₂ flow of 0.3 sccm (standard cubic centimeters per minute), yields an active N flux ϕ_N of 0.275 ± 0.05 ML/s as determined by the thickness of layers grown under Ga-rich conditions (in the following, a ML refers to the areal density of either the Ga or the N surface sites on GaN(1 $\bar{1}00$), i.e., 1.21×10^{15} cm⁻²). The Ga flux ϕ_{Ga} was determined by the thickness of layers grown under (slightly) N-rich conditions at a temperature of 580 °C where Ga desorption can be neglected. This procedure is possible only in a limited range of Ga fluxes (0.2–0.5 ML/s), outside of which it was determined by the vapor pressure of Ga fit to the experimentally obtained values for the absolute flux. The substrate temperature was calibrated by the visual observation of the melting point of Al attached to the SiC substrate. The growth front was monitored *in situ* by RHEED at 20 kV energy and an incidence angle of 1.5°. The diffraction patterns along all major azimuths of GaN(1 $\bar{1}00$), i.e., [1 $\bar{1}20$] (0°), [2 $\bar{2}43$] ($\approx 39^\circ$), [1 $\bar{1}23$] ($\approx 58^\circ$), and [0001] (90°),²¹ were recorded using a charge-coupled device (CCD) camera. The intensity of the specular spot and other regions of interest are recorded using a digital RHEED analysis system,²² which was set to sample data at a rate of 25 Hz. All recorded RHEED transients are corrected for the background and normalized to unity.

On-axis ($\pm 0.5^\circ$), [100]-oriented γ -LiAlO₂ (LAO) grown by a modified Chrochalzki technique was used as substrate.¹⁸ The wafers were chemomechanically polished to a root-mean-square roughness of 0.2 nm.²³ The as-received wafers were degreased sequentially in trichlorethylene (10 min), acetone (5 min), and methanol (5 min) in an ultrasonic bath. Finally, the substrate was dipped (30–60 s) in deionized water (DI H₂O). The cleaned LAO wafer was fixed with In onto a Si substrate which was then clipped to a Mo holder. Prior to growth, the substrate was outgassed in the load-lock chamber for 1 h at 200–300 °C. Growth was initiated by nucleation at 580 °C under Ga-rich conditions.²¹ The growth temperature was then raised to 740 °C and kept constant during the subsequent adsorption/desorption studies and growth. All of these studies have been done using a 500 nm thick GaN(1 $\bar{1}00$) film grown under standard conditions, i.e., Ga-stable growth ($\phi_{Ga}=0.475$ ML/s, $\phi_N=0.275$ ML/s) and a substrate temperature of 740 °C.

III. RESULTS

In the course of our previous work, we have noted that the smoothest layers exhibited a complex RHEED pattern when the surface was quenched to about 150 °C with a cooling rate of 40 °C/min and the N flux switched off (plasma extinguished) immediately at the termination of growth.²¹ The RHEED pattern observed exhibits a fourfold periodicity along all major azimuths, consistent with a (4 \times 4) reconstruction with respect to the unit mesh of the GaN(1 $\bar{1}00$) surface. Note that this reconstruction is not identical to the pseudo-(4 \times 5) reported by Lee *et al.*,²⁰ which gave rise to a fourfold pattern along the [0001] azimuth only. In the fol-

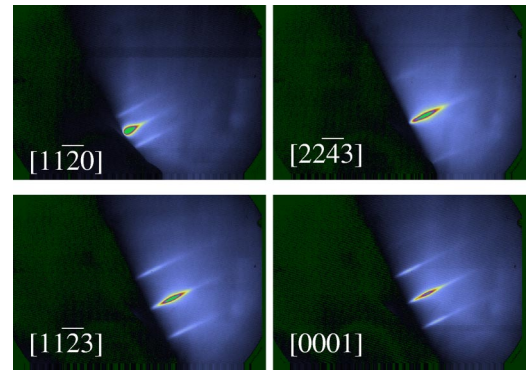


FIG. 1. (Color online) RHEED patterns of the GaN(1 $\bar{1}00$) film, recorded during growth at 740 °C along the major azimuths of GaN(1 $\bar{1}00$) as indicated.

lowing, we establish a relation between the adsorbed Ga coverage and reconstructions of the surface.

A. Relation between Ga coverage and surface reconstructions

Figure 1 shows the characteristic (1 \times 1) RHEED pattern observed during growth of *M*-plane GaN under the conditions given above. The pattern is entirely streaky, but dim, very similar to the RHEED pattern observed during growth of *C*-plane GaN. Upon interrupting the growth for about 20 s at constant temperature with the N flux on, the intensity of the pattern increases greatly, while the (1 \times 1) symmetry does not change. This recovery behavior is related to the desorption of a Ga adlayer, as will be discussed in detail in Sec. III B.

The RHEED pattern of the recovered surface does not exhibit any appreciable change when switching the N flux off. It does not change either when subsequently cooling the sample down to 100 °C. Upon deposition of up to 4 ML of Ga on this surface at 100 °C, the only noticeable change is that the RHEED pattern becomes dim similar to that observed during growth (cf. Fig. 1). This finding is in marked contrast to the observation of a (4 \times 4) reconstruction for the surface quenched to low temperature immediately after growth. Apparently, the thermal energy at 100 °C is insufficient for the Ga adatoms to condense into this reconstruction.

To study the formation of the (4 \times 4) reconstruction further with this sample, the excess Ga deposited at 100 °C is first flashed off by heating the sample to 740 °C, leaving a Ga terminated surface that is virtually identical to that observed during growth interruptions. The sample is next cooled down to 580 °C, at which the desorption of Ga is negligible. Next, we deposit 1 ML of Ga onto this surface. Upon cooling to 100 °C, clear half-order streaks are observed along all azimuths except for [1 $\bar{1}20$], consistent with a (1 \times 2) reconstruction of GaN(1 $\bar{1}00$). Upon heating, the half-order streaks abruptly disappear at a temperature of 250 °C, but the pattern stays dim in comparison to that of the recovered surface. An additional ML of Ga is then deposited at 580 °C, which gives rise to a more intense (1 \times 2) reconstruction after cooling to 100 °C as shown in Fig. 2. However, we often observe the formation of 1/4-order streaks

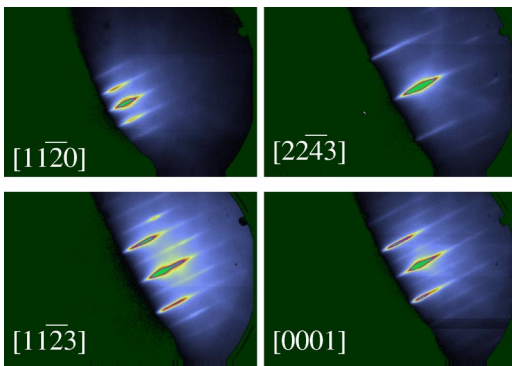


FIG. 2. (Color online) RHEED patterns of the GaN($1\bar{1}00$) film, recorded at 100°C after a two-step deposition of 2 ML Ga at 580°C along the major azimuths of GaN($1\bar{1}00$) as indicated. Note the intense half-order streaks along all azimuths except for $[1\bar{1}\bar{2}0]$.

[i.e., next to the (00) streak] along the $[1\bar{1}\bar{2}0]$ azimuth at this coverage, which would indicate a (4×2) reconstruction. Note that we never observe an indication of fractional-order streaks along any azimuths other than $[1\bar{1}\bar{2}0]$ at this coverage. A superposition of (1×2) and (4×4) reconstructed domains should give rise to $1/4$ -order streaks along all azimuths, and we thus believe that this observation rather results from a chainlike ordering of (1×2) -reconstructed domains.

The sample is then heated to 580°C again. Finally, the procedure is repeated for the deposition of an additional ML of Ga, resulting in a total of 3 ML of Ga on the surface. Figure 3 shows the resulting RHEED pattern, which exhibits an intense (4×4) reconstruction identical to that observed when quenching the sample after growth under standard conditions.

We have checked that the deposition of 2 and 3 ML of Ga in one step at 580°C results in RHEED patterns which are indistinguishable from those displayed in Figs. 2 and 3, respectively. Deposition of intermediate amounts, such as 2.5 ML, results in a fourfold periodicity along $[1\bar{1}\bar{2}0]$, but a twofold along all other azimuths, i.e., the (4×2) reconstruction mentioned above. Deposition of larger amounts than 3

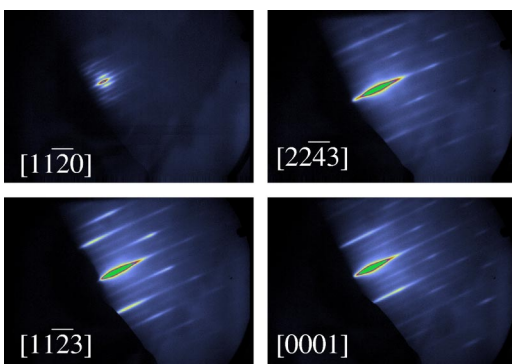


FIG. 3. (Color online) RHEED patterns of the GaN($1\bar{1}00$) film, recorded at 100°C after a three-step deposition of 3 ML Ga at 580°C along the major azimuths of GaN($1\bar{1}00$) as indicated. Note the intense quarter-order streaks along all azimuths.

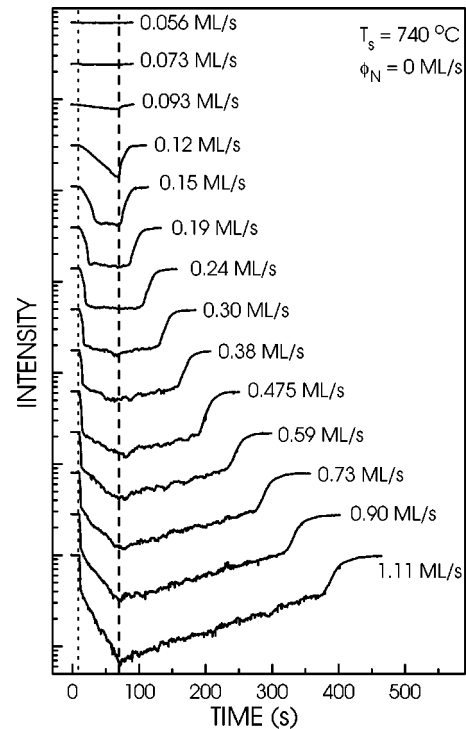


FIG. 4. Variation of the specular RHEED intensity in vacuum (i.e., $\phi_N=0$) upon adsorption of Ga for 60 s and subsequent desorption for a substrate temperature T_s and Ga fluxes as indicated. The individual transients are vertically shifted for clarity. The dotted line at $t=10$ s indicates the opening, the dashed line at $t=70$ s the closing of the Ga shutter.

ML reduces the overall intensity of the pattern, but does not change its symmetry. In all cases, the quarter-order streaks get diffuse and eventually disappear at temperatures above 250°C .

It is clear from these experiments that Ga adlayers at two distinct coverages exist, which condense at low temperatures into a $(1\times 2)/(4\times 2)$ reconstruction at bilayer coverage and a (4×4) reconstruction at trilayer coverage. On surfaces with intermediate amounts of adsorbed Ga, both reconstructions may coexist (presumably in the form of domains) although we have no experimental evidence for such a coexistence.

B. Ga adsorption/desorption kinetics

The recovery behavior of the surface at elevated temperatures provides the opportunity to study the adsorption/desorption kinetics of Ga in real time. For the following experiments, the sample was held at a constant temperature of 740°C either in vacuum or exposed to an active N flux of 0.275 ML/s. Ga adsorption/desorption isotherms were recorded by monitoring the intensity of the specularly reflected beam along the $[22\bar{4}3]$ azimuth, starting with 60 s of adsorption and allowing the surface to recover completely prior to the next experiment.

Figure 4 shows the variation of the specular RHEED intensity I_s for Ga fluxes between 0.056 and 1.11 ML/s. For the two lowest fluxes, no appreciable change in the RHEED

intensity is observed, reflecting that Ga desorption at this temperature inhibits the adsorption of significant amounts of Ga on the surface. At higher fluxes (0.12 ML/s), the RHEED intensity exhibits a clear drop once Ga deposition is initiated, and an immediate recovery once the Ga supply is stopped. For $\phi_{\text{Ga}}=0.15$ and 0.19 ML/s, the RHEED intensity stabilizes after the initial drop, and recovers without (0.15 ML/s) or with a very short (0.19 ML/s) delay. Apparently, this situation corresponds to a balance between impinging and desorbing Ga flux, thus establishing a steady-state Ga coverage at the surface independent of deposition time. For a Ga flux higher than this value, the recovery is progressively delayed. Furthermore, the RHEED intensity continues to decrease after the initial, rapid drop, albeit at a much slower rate.

Guided by the well understood Ga adsorption/desorption kinetics on the GaN(0001) surface,^{13–17} we interpret these observations according to the following four-stage scenario. Initially (stage I), Ga adsorbs in a layer-by-layer fashion, resulting in the initial, rapid drop of the RHEED intensity until full coverage is established. If the impinging Ga flux exceeds the desorbing flux, Ga accumulation takes place, eventually leading to the formation of droplets which manifests itself in a further but slower decrease of the RHEED intensity (stage II). Once the Ga supply is stopped, the Ga adlayer (the exact coverage of which we will attempt to determine below) starts to desorb. Excess Ga, however, acts as reservoir, thus stabilizing the Ga adlayer and delaying recovery (stage III). Once the excess Ga is depleted, the Ga adlayer desorbs, accounting for the rapid final recovery (stage IV).

Figure 5 shows the variation of the specular RHEED intensity I_s for Ga fluxes between 0.19 and 1.66 ML/s with an additional active N flux of 0.275 ML/s. The behavior observed is analogous to that in Fig. 4, and we thus interpret it in the same way. Particularly, the intensity right after stage I and just prior to stage IV are independent on Ga flux once ϕ_{Ga} is larger than 0.48 ML/s, essentially identical to the case of Ga adsorption in vacuum. We take this as a confirmation that a stable Ga adlayer coverage is formed also under an active N flux, i.e., during growth.

To analyze these Ga isothermal transients quantitatively, we next define parameters associated with the four stages of Ga adsorption/desorption introduced above. Figure 6 visualizes the relation between these parameters to the RHEED transients for the example of $\phi_{\text{Ga}}=0.73$ ML/s. The time interval required for the completion of stage i is denoted by t_i , while I_i refers to the intensity at the end of this stage. While the time intervals t_1-t_3 are well defined (note that $t_2=60-t_1$), no such interval can be defined unambiguously for stage IV. In fact, plotting $\ln(1-I_s)$ reveals the desorption process in this stage to be exponential, thus being characterized by a time constant τ_4 rather than by a time interval. We will analyze stage IV in context with a quantitative description of these transients in Sec. IV.

Apart from the lowest Ga fluxes used here, where full coverage cannot be reached, I_1 is found to be independent of the Ga flux for both Ga adsorption/desorption in vacuum and under an active N flux. This finding confirms the view that stage I is related to the adsorption of a fixed amount of Ga.

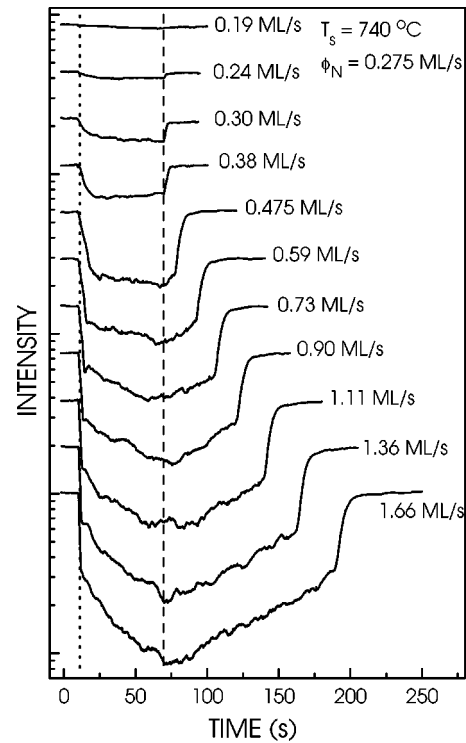


FIG. 5. Variation of the specular RHEED intensity under an active N flux ($\phi_{\text{N}}=0.275$ ML/s) upon adsorption of Ga for 60 s and subsequent desorption for a substrate temperature T_s and Ga fluxes as indicated. The individual transients are vertically shifted for clarity. The dotted line at $t=10$ s indicates the opening, the dashed line at $t=70$ s the closing of the Ga shutter.

The same applies to I_3 , which is found to be identical to I_1 within experimental uncertainty. Stage IV thus indeed corresponds to the desorption of a fixed amount of Ga, and this amount seems to be identical to that adsorbed during stage I.

Figure 7 depicts the adsorption time interval t_1 as function of ϕ_{Ga} . We see that this quantity exhibits the intuitively expected inverse proportionality to ϕ_{Ga} . The fits shown by the solid lines are based on the simple assumption that the

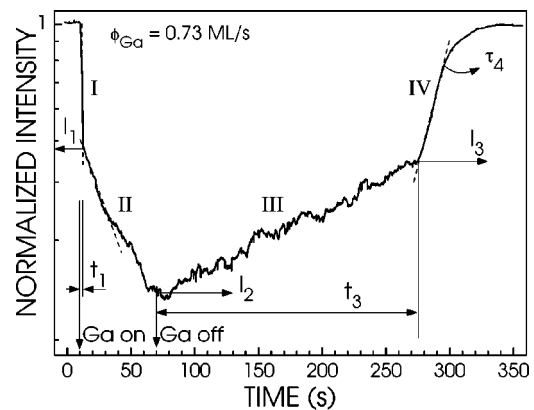


FIG. 6. Definition of the parameters used for analyzing the RHEED transients for the example of $\phi_{\text{Ga}}=0.73$ ML/s. The roman numerals denote the respective stage of the Ga adsorption/desorption process.

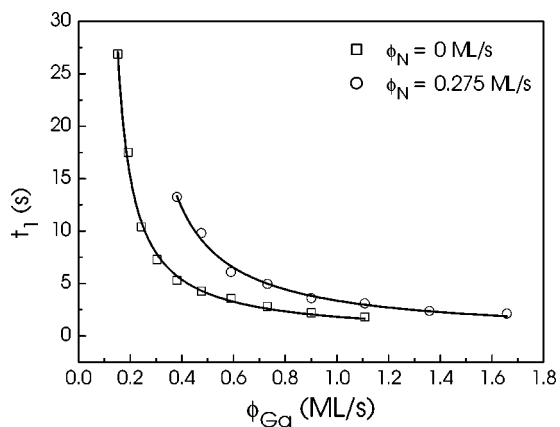


FIG. 7. t_1 vs Ga flux for adsorption in vacuum (\square) and under an active N flux (\circ). The solid lines are fits as discussed in the text.

Ga coverage θ is given by the product of t_1 and the Ga flux ϕ_{Ga} , minus the product of t_1 and the sum of a mean desorption ($\bar{\phi}_{\text{des}}$) and consumption flux ($\bar{\phi}_{\text{N}}$), i.e., $t_1 = \theta / (\phi_{\text{Ga}} - \bar{\phi}_{\text{des}} - \bar{\phi}_{\text{N}})$, with $\bar{\phi}_{\text{N}}$ being nonzero in the presence of active N. Note that these quantities are not to be confused with the actual desorption rate and the (N-limited) growth rate at full adlayer coverage. Both desorption rate and growth rate depend on the adlayer coverage and tend to zero for zero coverage. For first-order kinetics ($\bar{\phi} = \gamma\theta$, where γ denotes the actual rate and θ the coverage), the mean quantities introduced above correspond to half the actual rates.

The good agreement between this expression and the experimentally measured values for t_1 confirms that the amount of Ga adsorbed in stage I is indeed constant for a Ga flux resulting in a complete Ga adlayer coverage. Quantitatively, the fit returns values $\theta = 1.62$ ML and $\bar{\phi}_{\text{des}} = 0.09$ ML/s in vacuum, and $\theta = 2.78$ ML and $\bar{\phi}_{\text{des}} + \bar{\phi}_{\text{N}} = 0.17$ ML/s under an active N flux. The coverage obtained for adsorption under an active N flux is significantly higher than that obtained for the vacuum adsorption, and the difference is far beyond any possible error margin. Let us stress, however, that this approach is at best a rough approximation, as it is based on the implicit assumption that both the adsorption and the desorption processes are independent of coverage. We will analyze this situation in Sec. IV in more detail.

A quantity that can be determined at the present stage without ambiguity is the amount of Ga impinging onto the surface, which is given simply by $t_1 \phi_{\text{Ga}}$. Figure 8 shows the impinging amount of Ga during t_1 as a function of the Ga flux for both adsorption in vacuum and under an active N flux. For the lowest fluxes, this amount is vastly overestimated since this analysis neglects desorption altogether. For higher fluxes, the amount is constant as indicated by the solid lines.

For adsorption in vacuum, this amount corresponds to 2.04 ± 0.02 ML. As we will show in Sec. IV, this value closely corresponds to the actually adsorbed amount since Ga desorbing from the adlayer is replaced by excess Ga at these high Ga fluxes. In fact, the above view that excess Ga forms only after completion of the Ga adlayer is overly sim-

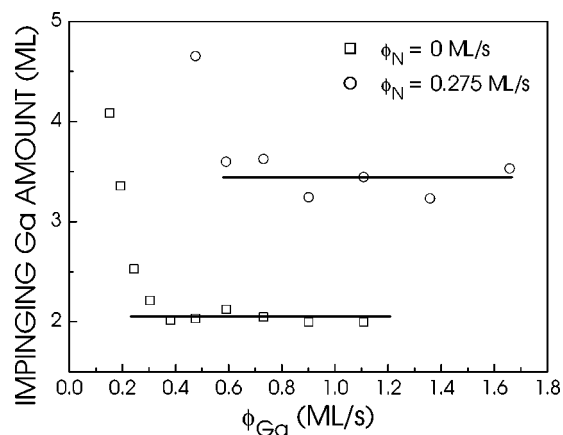


FIG. 8. Amount of impinging Ga during stage I as obtained from t_1 vs Ga flux in vacuum (\square) and under an active N flux (\circ). The solid lines are fits of the data with a constant.

plistic, since an infinite diffusion rate of the excess Ga adatoms would be required for this strict separation. The same statement applies to the entire depletion of excess Ga at the onset of stage IV.

For adsorption under an active N flux, we find that this amount is as large as 3.45 ± 0.07 ML for Ga fluxes higher than 0.4 ML/s. The active N flux cannot reduce this amount to a bilayer as found for vacuum conditions. We thus believe that these results are significant in that they indicate a stabilization of a larger Ga adlayer coverage by the active N flux compared to vacuum adsorption. It is possible that the two different surface reconstructions, one occurring at bilayer, the other at trilayer coverage, are related to this finding.

A further indication for the formation of a dynamically stable Ga adlayer is provided by the dependence of the intensity I_2 on Ga flux. For adsorption in vacuum and a Ga flux between 0.15 and 0.24 ML/s, I_2 is found to be constant, implying there is only little, if any, accumulation of excess Ga occurring in this range. Note that one should not expect an entirely constant intensity here, which is often postulated to be a signature of a dynamic equilibrium. For kinetically controlled conditions, an increase of the Ga flux will slightly but inevitably shift the stoichiometry to the more Ga-rich side. However, for higher fluxes, I_2 abruptly drops signifying the formation of significant amounts of excess Ga under these conditions. The precarious balance between adsorption and desorption is thus eventually broken.

The last quantity which is related to full Ga adlayer coverage is the recovery time interval t_3 . According to our interpretation, this time interval is determined primarily by the desorption of the adlayer coverage, provided that the diffusion rate of excess Ga replenishing the Ga adlayer is sufficiently high. Figure 9 shows t_3 as a function of the Ga flux for both vacuum conditions and under an active N flux. For the former case, the linear fits shown by the dashed and solid lines are based on the assumption that the excess Ga coverage n built up during stage II is effectively reduced by substitution of the desorbing Ga adlayer coverage in stage III. In other words, $t_3 = n / \phi_{\text{des}}^{\text{max}}$, where $\phi_{\text{des}}^{\text{max}}$ is the desorption flux for full Ga adlayer coverage. Since n accumulates during

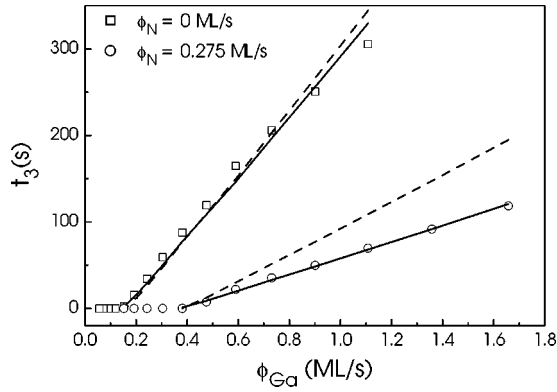


FIG. 9. t_3 vs Ga flux in vacuum (\square) and under an active N flux (\circ). The dashed and solid lines show linear fits to the data as discussed in the text.

time t_2 where full coverage is already established for Ga fluxes higher than 0.15 ML/s, we may write $n = t_2(\phi_{\text{Ga}} - \phi_{\text{des}}^{\text{max}})$. This simple approximation, which implicitly assumes that all excess Ga is available for substituting the Ga adlayer, is shown by the dashed line and returns a maximum desorption flux of 0.16 ML/s. If we take into account that the diffusion rate of excess Ga is not infinite, and thus only a certain fraction a of the excess Ga coverage is available for substituting the Ga adlayer, we may express n phenomenologically as $n = at_2(\phi_{\text{Ga}} - \phi_{\text{des}}^{\text{max}})$. The result of this consideration is the solid line, a fraction $a = 0.84$ and a desorption flux of 0.143 ML/s.

For the case of recovery under an active N flux, we proceed exactly in the same way as described above, except for the fact that we also consider the consumption flux (equal to the growth rate) due to the presence of active N: $t_3 = n/(\phi_{\text{des}}^{\text{max}} - \phi_{\text{con}}^{\text{max}})$, where $n = at_2(\phi_{\text{Ga}} - \phi_{\text{des}}^{\text{max}} - \phi_{\text{con}}^{\text{max}})$. When explicitly assuming that the diffusion rate of the excess Ga coverage is infinite ($a = 1$), we do not get any acceptable fit (dashed line in Fig. 9). Considering, as above, that only a fraction a of the excess Ga is able to replenish the Ga adlayer, we obtain the solid line, $a = 0.59$, and $\phi_{\text{des}}^{\text{max}} + \phi_{\text{con}}^{\text{max}} = 0.365$ ML/s. Given that the N flux has been determined to be 0.275 ML/s, the latter result indicates a desorption flux at full adlayer coverage of 0.09 ML/s, considerably less than in vacuum. This result is in good agreement with that obtained from the analysis of t_1 (cf. Fig. 7).

To summarize this section, our analysis indicates a stable Ga coverage slightly below 2 ML in vacuum. Larger coverages result in the formation of excess Ga. Under an active N flux, the stable coverage obtained is close to 3 ML. This analysis, however, neglects the interaction between the Ga adlayer and excess Ga. We will show in Sec. IV that the actual coverage is close to the amount of Ga delivered to the surface during the adsorption interval t_1 , which is one bilayer for adsorption in vacuum, and a trilayer under an active N flux.

IV. KINETIC MODEL

We have seen in the preceding sections that the strict distinction between the formation of a Ga adlayer and the sub-

sequent accumulation of excess Ga is too simplistic. The most important questions we must ask are thus, if the four-stage scenario developed in Sec. III B is essentially correct, and how accurate the approximate analyses presented above actually are.

To answer this question, we next develop a quantitative model of our interpretation. The model is required to account for adsorption and desorption of Ga as well as for the formation of excess Ga interacting with the Ga adlayer, and for GaN growth in the case of the simultaneous presence of Ga and N. Our model, in units normalized to the maximum Ga adlayer coverage, is described by the equations

$$\frac{d\theta}{dt} = j_{\text{Ga}}(1 - \theta) + d_{\text{Ga}}(1 - \theta)n - \gamma_{\theta}\theta - j_{\text{N}_2}\theta, \quad (1)$$

$$\frac{dn}{dt} = j_{\text{Ga}}\theta - d_{\text{Ga}}(1 - \theta)n - \gamma_n n, \quad (2)$$

where θ denotes the Ga adlayer coverage, n the amount of excess Ga, j_{Ga} and j_{N} the Ga and N delivery rate, d_{Ga} the diffusion rate of excess Ga adatoms impinging onto θ , and γ_{θ} (γ_n) the rates of Ga adlayer (excess Ga) desorption. The first term of each equation accounts for adsorption of Ga, building up the Ga adlayer θ and subsequently excess Ga n . In much the same way, the second terms account for diffusion of excess Ga impinging onto the Ga adlayer. The third terms describe the desorption of θ and n . The last term in Eqs. (1), finally, stands for the incorporation of Ga and N adatoms into the crystal, i.e., actual growth. Note that the model described by Eqs. (1) and (2) is a linearized, and highly simplified version of microscopic theories of surface kinetics such as developed in Ref. 24. This simplification is necessary to reduce the number of free parameters and thus to guarantee stable fits, but also means that, while our model is perhaps the simplest one accounting for the phenomena we wish to describe, there certainly are a variety of more refined models which could equally well describe the data.

Finally, we have to relate the surface coverage calculated by means of Eqs. (1) and (2) to the quantity experimentally observed, namely, the RHEED intensity. Since the Ga adlayer at growth temperature does not condense into a reconstruction, but rather represents a liquid, it manifests itself in an attenuation of the RHEED intensity. We thus follow the well-established relation between surface coverage and intensity in Auger attenuation experiments,²⁵ which reads

$$I(\theta, n) = e^{-\theta - bn}. \quad (3)$$

Both the adlayer coverage θ and the excess coverage n are assumed to attenuate the intensity exponentially. The ripening of excess Ga to clusters and droplets leads to a (geometrically determined) different rate of decrease with respect to the Ga adlayer coverage, as expressed by the prefactor b . Since b is assumed to be constant, the model does not describe the ripening dynamics.

Figure 10 shows three experimental Ga adsorption/desorption isotherms in vacuum together with simulations based on Eqs. (1)–(3). Except for the Ga flux, which was taken to be equal to the experimentally determined flux as

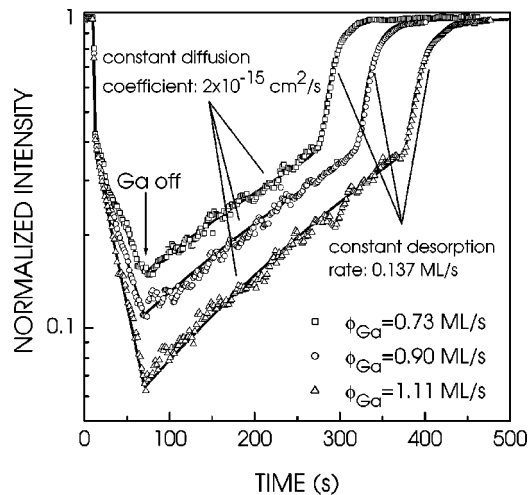


FIG. 10. Experimental (symbols) and simulated (solid lines) RHEED transients for three different Ga fluxes as indicated in the figure. For clarity, only each 40th datapoint is displayed.

indicated in the figure, we used the same parameters for these simulations, namely: a diffusion coefficient of $2 \times 10^{-15} \text{ cm}^2/\text{s}$, a Ga adlayer desorption flux of 0.137 ML/s , an excess Ga desorption flux of 0.003 ML/s , and a prefactor b of 0.06 ± 0.003 . Evidently, the agreement between the experimental transients and the simulations is very good. Most importantly, this agreement can only be obtained with the above set of parameters, since the slope of the transient in stage III is mainly determined by γ_n , while γ_θ determines the slope of the transient in stage IV. Furthermore, the onset of stage IV depends essentially on the sum of γ_n and γ_θ , resulting in unique fits to the experimental data. This result confirms that our general understanding of the adsorption/desorption processes is essentially correct. Of particular interest at this point are thus the Ga adlayer and excess Ga coverages predicted by the simulation at the intensities I_1 and I_3 . At I_1 , these coverages are found to be independent of Ga flux for $\phi_{\text{Ga}} \geq 0.15 \text{ ML/s}$, and amount to $\theta = 1.64 \text{ ML}$ and $n = 0.42 \text{ ML}$, respectively. At I_3 , we obtain $\theta = 1.86 \text{ ML}$ and $n = 0.34 \text{ ML}$, again independent of Ga flux for $\phi_{\text{Ga}} \geq 0.15 \text{ ML/s}$. The coexistence of θ and n is a direct result of the finite diffusion rate of the excess Ga, as already concluded above.

An interesting detail is the inability of our model to accurately fit stage I and the transition towards stage II, as shown for a Ga flux of 0.9 ML/s in Fig. 11. The experimental transients exhibit two clearly distinct slopes during stage I, an abrupt change of slope at the transition to stage II, and a gradual change of slope thereafter. It is likely that this complex behavior reflects the formation of the bilayer by the subsequent adsorption of a lower and upper ML, accompanied by the simultaneous nucleation and diffusion of excess Ga on both of these levels. Our model as formulated above is obviously unable to reproduce this process, since it does not distinguish the two distinct layers of the Ga bilayer but treats them as being one entity.

However, there are other factors which must be considered as well in this context. If the Ga adlayer is not com-

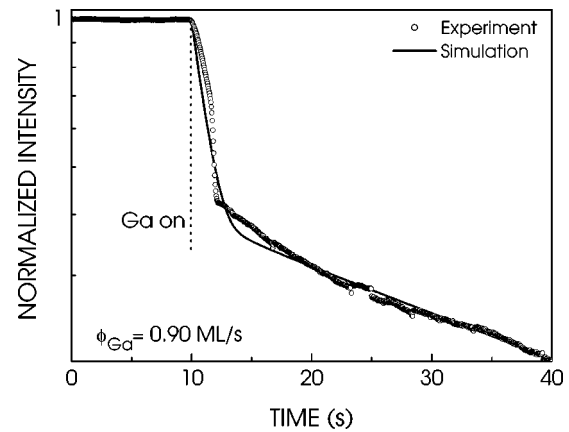


FIG. 11. Experimental (symbols) and simulated (solid lines) RHEED transient for the indicated Ga flux during the initial adsorption stage.

pleted ($\theta < 1$), it does not form a continuous film but two-dimensional islands. This inevitable fact has several important consequences. First of all, our model treats θ as a continuous variable, and neglects its inherently discrete nature at low coverages. Second, the desorption kinetics of two-dimensional islands is known to be dominated by desorption from the islands' edges, which changes the first-order (monomolecular) desorption kinetics assumed here ($\propto \theta$) to half-order ($\propto \sqrt{\theta}$). Third, the desorption rate γ_θ will be enhanced in this case, essentially resulting in a coverage-dependent desorption rate which is no longer a constant but a function of θ . In fact, for Ga fluxes lower than 0.19 ML/s , we had to increase γ_θ significantly to account for the early and comparatively rapid recovery observed. In view of that said above, it is clear that this simple measure is purely phenomenological and only approximates the actual desorption process.

We next turn to a comparison between experimental Ga adsorption/desorption isotherms under active N flux and simulations based on Eqs. (1)–(3). As above, we take the experimentally determined Ga flux for the simulations, and, of course, the additional N flux. For a Ga flux larger than 0.475 ML/s , the parameters required to get a good agreement between simulated and experimental transient are identical to those given above, except for γ_θ , which turns out to be slightly larger (0.155 ML/s). For lower Ga fluxes, the Ga adlayer is not completed and γ_θ increases drastically as discussed above for the case of desorption in vacuum. Figure 12 shows the three RHEED transients at the transition between N-stable and Ga-stable conditions. The desorption fluxes required to fit them are 0.155 , 0.21 , and 0.28 ML/s from low to high Ga flux. The good agreement between experimental and simulated transients shows that the adsorption/desorption kinetics is not fundamentally different in the presence of a N flux compared to that under vacuum. Rather, the N flux seems merely to consume Ga and thus to shift the adsorption/desorption balance toward higher Ga fluxes.

For sake of completeness, we determine again the Ga adlayer and excess Ga coverages predicted by the simulation at I_1 and I_3 . At I_1 , these coverages are found to be independent of Ga flux for $\phi_{\text{Ga}} \geq 0.475 \text{ ML/s}$, and amount to θ

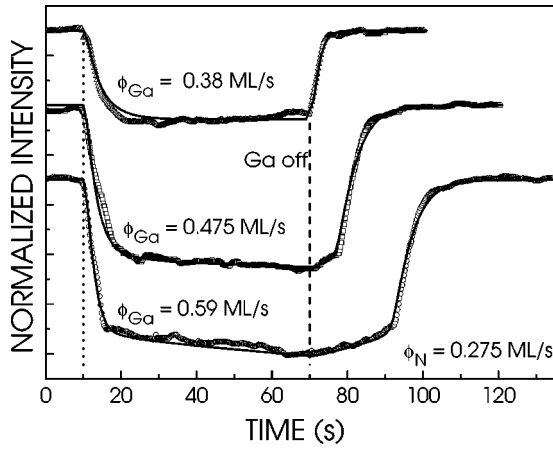


FIG. 12. Experimental (symbols) and simulated (solid lines) RHEED transients for three different Ga fluxes as indicated in the figure and an active N flux of 0.275 ML/s. The transients are vertically offset for clarity. The Ga opening and closing are indicated by dotted and dashed lines, respectively.

= 1.94 ML and $n = 0.88$ ML, respectively. At I_3 , we obtain $\theta = 1.88$ ML and $n = 0.26$ ML, again independent of Ga flux for $\phi_{Ga} \geq 0.475$ ML/s. The high coverage at I_1 is consistent with that deduced from Fig. 7.

At this point, it is instructive to examine the predictions of our model for prolonged growth using the parameters used

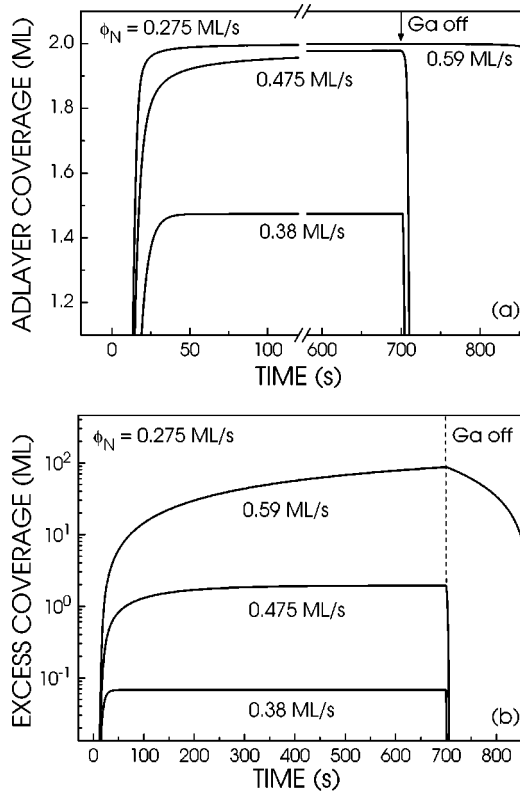


FIG. 13. Simulated Ga adlayer and excess Ga coverage during growth. The parameters used are those deduced from the simulations shown in Fig. 12, but the Ga supply is now terminated at $t = 700$ s.

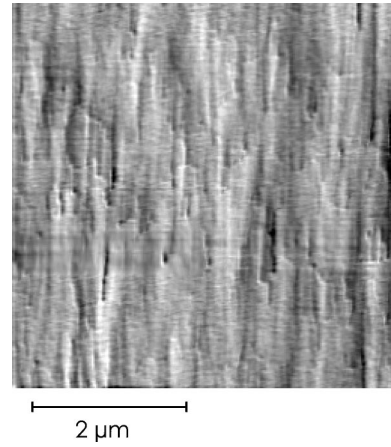


FIG. 14. AFM micrograph of a 500 nm-thick GaN($1\bar{1}00$) layer grown under standard conditions. The vertical stripes are oriented along $[11\bar{2}0]$. The peak-to-valley and root-mean-square roughness of this layer are 6.6 and 0.6 nm over the mapped area of $5 \times 5 \mu\text{m}^2$, respectively.

for the simulations in Fig. 12. Figure 13(a) shows the Ga bilayer coverage vs growth time for the three different Ga fluxes at the transition between N-stable and Ga-stable conditions. As expected, full bilayer coverage is not reached for the lowest Ga flux. In contrast, the Ga adlayer coverage slowly converges towards a full bilayer for the intermediate Ga flux, and is obtained rapidly for the highest Ga flux. However, as shown in Fig. 13(b), the price one pays for this rapid bilayer completion is a diverging Ga excess coverage, which increases without bound for prolonged growth. In fact, layers grown under these conditions exhibit a high density of Ga droplets and, after HCl etching, of corresponding surface defects. In contrast, the Ga excess coverage saturates at 2 ML for the intermediate Ga flux, reflecting that a dynamic equilibrium is established under these conditions. Note that the desorption flux for this case is 0.21 ML/s, which in fact is almost exactly equal to the difference of Ga and N flux. The total Ga coverage during growth is here thus 4 ML, which is consistent with the observation of the Ga-trilayer related (4×4)-reconstruction observed for this growth conditions after quenching the sample to 100°C (cf. Fig. 3). For the lowest Ga flux, the excess coverage is (as expected) negligible.

Finally, Fig. 14 shows an atomic force microscopy (AFM) image of a GaN($1\bar{1}00$) layer grown under our standard conditions, which has been deemed previously to be most suitable on empirical grounds.²¹ In particular, these conditions result in droplet-free and microscopically smooth surfaces. The surface of the layer exhibits the characteristic highly anisotropic, striplike morphology of GaN($1\bar{1}00$) layers.^{19,4,20} With a root-mean-square roughness of 0.6 nm, the smoothness of this layer approaches (but does not yet reach) that of state-of-the-art GaN(0001) layers grown by MBE.

V. CONCLUSIONS

We have studied the adsorption and desorption kinetics of Ga on GaN($1\bar{1}00$) using *in situ* reflection high-energy elec-

ron diffraction. Two stable surface phases were identified, which manifest themselves at low temperatures by a $(1 \times 2)/(4 \times 2)$ reconstruction at bilayer coverage and a (4×4) reconstruction at trilayer coverage. This behavior is quite different from that observed on GaN(0001), for which the Ga bilayer does not give rise to any observable surface reconstruction even at room temperature. We furthermore do not observe the bilayer-related sidebands frequently seen on GaN(0001), which are attributed to the lateral contraction of the topmost adlayer. Apparently, the Ga adlayer on GaN(1 $\bar{1}$ 00) is more strongly bonded compared to that on GaN(0001), since it gives rise to a reconstruction with sharp and distinct fractional-order reflections and stays commensurate to GaN.

At high temperature, Ga adsorbs layer-by-layer up to a certain coverage after which condensation of excess Ga occurs which eventually ripens into Ga droplets. The total coverages determined for adsorption in vacuum and under N flux are distinctly different, and correspond to bilayer coverage in vacuum and trilayer coverage under an active N flux, respectively. This finding is a consequence of the fact that the additional N flux shifts the adsorption/desorption balance towards more Ga-rich conditions. In both cases, the bilayer

desorption is counteracted by “feeding” from excess Ga. This process is efficient thanks to a relatively large diffusion rate of the excess Ga, and growth interruptions thus largely deplete the excess Ga while keeping the bilayer intact. Finally, the optimum growth conditions with regard to surface morphology are those giving rise to trilayer coverage at low temperature. Under these conditions, the Ga adlayer coverage converges towards 2 ML, and the excess coverage saturates at a comparable amount. Compared to GaN(0001), these optimum growth conditions correspond to slightly more Ga-rich conditions. In our case, we establish these conditions by a growth temperature which is $\approx 20^\circ\text{C}$ lower than that for GaN(0001).

ACKNOWLEDGMENTS

The authors gratefully acknowledge technical assistance from Hans-Peter Schönherr and Doris Spaniol. We are indebted to Randall Feenstra (Carnegie Mellon University) for valuable discussions, and to Vladimir Kaganer, Patrick Waltereit (University of California at Santa Barbara), and Glenn Solomon (Stanford University) for critical reading of the manuscript.

*Electronic address: brandt@pdi-berlin.de

¹P. Waltereit, O. Brandt, A. Trampert, H.T. Grahn, J. Menniger, M. Ramsteiner, M. Reiche, and K.H. Ploog, *Nature (London)* **406**, 865 (2000).

²S. Ghosh, P. Waltereit, O. Brandt, H.T. Grahn, and K.H. Ploog, *Phys. Rev. B* **65**, 075202 (2002).

³S. Ghosh, O. Brandt, H.T. Grahn, and K.H. Ploog, *Appl. Phys. Lett.* **81**, 3380 (2002).

⁴C.Q. Chen, M.E. Gaevski, W.H. Sun, E. Kuokstis, J.P. Zhang, R.S.Q. Fareed, H.M. Wang, J.W. Yang, G. Simin, M.A. Khan, Herbert-Paul Maruska, David W. Hill, Mitch M.C. Chou, and Bruce Chai, *Appl. Phys. Lett.* **81**, 3194 (2002).

⁵E. Kuokstis, C.Q. Chen, M.E. Gaevski, W.H. Sun, J.W. Yang, G. Simin, M.A. Khan, H.-P. Maruska, D.W. Hill, M.C. Chou, J.J. Gallagher, and B. Chai, *Appl. Phys. Lett.* **81**, 4130 (2002).

⁶Y.J. Sun, O. Brandt, U. Jahn, T.Y. Liu, A. Trampert, S. Cronenberg, S. Dahr, and K.H. Ploog, *J. Appl. Phys.* **92**, 5714 (2002).

⁷Y.J. Sun, O. Brandt, S. Cronenberg, S. Dahr, H.T. Grahn, K.H. Ploog, P. Waltereit, and J.S. Speck, *Phys. Rev. B* **67**, 041306(R) (2003).

⁸Y.J. Sun, O. Brandt, M. Ramsteiner, H.T. Grahn, and K.H. Ploog, *Appl. Phys. Lett.* **82**, 3850 (2003).

⁹Y.J. Sun, O. Brandt, B. Jenichen, and K.H. Ploog, *Appl. Phys. Lett.* **83**, 5178 (2003).

¹⁰M.D. Craven, S.H. Lim, F. Wu, J.S. Speck, and S.P. DenBaars, *Appl. Phys. Lett.* **81**, 469 (2002).

¹¹H.M. Ng, *Appl. Phys. Lett.* **80**, 4369 (2002).

¹²W.H. Sun *et al.*, *Appl. Phys. Lett.* **83**, 2599 (2003).

¹³A.R. Smith, R.M. Feenstra, D.W. Greve, M.S. Shin, M. Skowronski, J. Neugebauer, and J.E. Northrup, *J. Vac. Sci. Technol. B* **16**, 2242 (1998).

¹⁴J.E. Northrup, J. Neugebauer, R.M. Feenstra, and A.R. Smith, *Phys. Rev. B* **61**, 9932 (2000).

¹⁵G. Mula, C. Adelman, S. Moehl, J. Oullier, and B. Daudin, *Phys. Rev. B* **64**, 195406 (2001).

¹⁶C. Adelman, J. Brault, D. Jalabert, P. Gentile, H. Mariette, G. Mula, and B. Daudin, *J. Appl. Phys.* **91**, 9638 (2002).

¹⁷C. Adelman, J. Brault, G. Mula, B. Daudin, L. Lymperakis, and J. Neugebauer, *Phys. Rev. B* **67**, 165419 (2003).

¹⁸P. Waltereit, O. Brandt, M. Ramsteiner, K.H. Ploog, R. Uecker, and P. Reiche, *J. Cryst. Growth* **218**, 143 (2000).

¹⁹P. Waltereit, O. Brandt, M. Ramsteiner, A. Trampert, H.T. Grahn, J. Menniger, M. Reiche, R. Uecker, P. Reiche, and K.H. Ploog, *Phys. Status Solidi A* **180**, 133 (2000).

²⁰C.D. Lee, R.M. Feenstra, J.E. Northrup, L. Lymperakis, and J. Neugebauer, *Appl. Phys. Lett.* **82**, 1793 (2003).

²¹Y.J. Sun, O. Brandt, and K.H. Ploog, *J. Vac. Sci. Technol. B* **21**, 1350 (2003).

²²SAFIRE by VTS Schwarz GmbH, Hindenburgstr. 12, D-76332 Bad Herrenalb, Germany.

²³CrysTec GmbH, Köpenickerstr. 325, D-12555 Berlin, Germany.

²⁴H.J. Kreuzer, in *Chemistry and Physics of Solid Surfaces VII*, edited by R. Vanselow and R.F. Howe (Springer, Berlin-Heidelberg, 1988), Vol. 7, p. 259.

²⁵M. Zinke-Allmann, *Surf. Sci. Rep.* **16**, 377 (1992).